HHS Public Access

Author manuscript

Microcirculation. Author manuscript; available in PMC 2018 August 01.

Published in final edited form as:

Microcirculation. 2017 August ; 24(6): . doi:10.1111/micc.12381.

Lymph node effective vascular permeability and chemotherapy uptake

Eelco F. J. Meijer[1,2], **Cedric Blatter**[2,3], **Ivy X. Chen**[1,2], **Echoe Bouta**[1,2], **Dennis Jones**[1,2], **Ethel R. Pereira**[1,2], **Keehoon Jung**[1,2], **Benjamin J. Vakoc**[2,3], **James W. Baish**[4], and **Timothy P. Padera**[1,2]

[1]Edwin L. Steele Laboratories for Tumor Biology, Department of Radiation Oncology, Massachusetts General Hospital Cancer Center, Boston, MA, USA

[2]Harvard Medical School, Boston, MA, USA

[3]Wellman Center for Photomedicine, Massachusetts General Hospital, Boston, MA, USA

[4]Department of Biomedical, Engineering, Bucknell University, Lewisburg, PA, USA

Abstract

Objective—Lymph node metastases are a poor prognostic factor. Additionally, responses of lymph node metastasis to therapy can be different from the primary tumor. Investigating the physiologic lymph node blood vasculature might give insight into the ability of systemic drugs to penetrate the lymph node, and thus into the differential effect of therapy between lymph node metastasis and primary tumors. Here, we measured effective vascular permeability of lymph node blood vessels and attempted to increase chemotherapy penetration by increasing effective vascular permeability.

Methods—We developed a novel three-dimensional method to measure effective vascular permeability in murine lymph nodes in vivo. VEGF-A was systemically administered to increase effective vascular permeability. Validated high-performance liquid chromatography protocols were used to measure chemotherapeutic drug concentrations in untreated and VEGF-A-treated lymph nodes, liver, spleen, brain, and blood.

Results—VEGF-A-treated lymph node blood vessel effective vascular permeability (mean 3.83 $\times 10^{-7}$ cm/s) was significantly higher than untreated lymph nodes (mean 9.87 $\times 10^{-8}$ cm/s). No difference was found in lymph node drug accumulation in untreated versus VEGF-A-treated mice.

Correspondence: Timothy P. Padera, Edwin L. Steele Laboratories for Tumor Biology, Department of Radiation Oncology, Massachusetts General Hospital Cancer Center, Boston, MA, USA. tpadera@steele.mgh.harvard.edu.

CONFLICT OF INTEREST

The authors declare that they have no competing interests.

Research was performed at the Edwin L. Steele Laboratories for Tumor Biology, Department of Radiation Oncology, Massachusetts General Hospital Cancer Center, Boston, Massachusetts 02114, USA.

SUPPORTING INFORMATION

Additional Supporting Information may be found online in the supporting information tab for this article.

Conclusions—Lymph node effective vascular permeability can be increased (~fourfold) by VEGF-A. However, no significant increase in chemotherapy uptake was measured by pretreatment with VEGF-A.

Keywords

chemotherapy; drug penetration; intravital microscopy; lymph node; vascular permeability

1 | INTRODUCTION

Solid tumors often metastasize to regional lymph nodes. This metastatic spread is a poor prognostic factor, regardless of the site of the primary tumor.[1] Systemic therapies are usually designed to treat the primary tumor, but it is known that the local tumor microenvironment alters the phenotypic behavior of cancer cells, including response to therapy.[2,3] Thus, therapies designed to treat primary tumors often are less efficacious in treating metastasis in their new microenvironment.[4,5] Because some patients show complete or partial responses in metastatic lymph nodes during chemotherapy,[6] it is assumed that these drugs are able to penetrate lymph nodes. However, disease recurrence in the lymph nodes of patients initially diagnosed without nodal metastasis or with nodal micrometastases is also common, suggesting systemic therapy does not eradicate these small pockets of cells. One difference between the macro- and micrometastatic settings is the ability of the tumor to alter the vasculature of the lymph node.[7] Investigation of the physiologic lymph node blood vasculature might therefore explain why systemic (intravenous) therapy fails to eradicate micrometastatic disease, which is when lymph node disease burden is lower and thus thought to be easier to treat. Systematic studies of chemotherapy drug penetration into lymph nodes—both under normal and disease conditions—could offer a better understanding of why there is a differential response of lymph node metastasis and primary tumors to therapy.

Published studies have looked at lymphoid tissue drug penetration in the context of HIV, as spleen, lymph nodes, and gut-associated lymphoid tissues have been identified as pharmacologic sanctuaries from antiretroviral therapy.[8,9] Also in HIV-infected patients, there is evidence that drug penetration into the lymph node is insufficient.[10–12] This likely contributes to HIV-infected T cells finding pharmacologic sanctuary in lymph nodes, which are then able to expand and repopulate the patient with infected cells after treatment is stopped.[10,13] Based on these data, we hypothesized that micrometastases and isolated metastatic cancer cells might similarly find pharmacologic sanctuary from chemotherapy. Employing validated methods to measure tissue drug concentrations, as well as our novel method to measure EVP in three dimensions,[14] we investigated whether low lymph node blood vessel EVP could play a role in the establishment of pharmacologic sanctuary sites for metastatic cancer cells, and whether enhancing blood vessel EVP using VEGF-A[15–17] could improve drug delivery. EVP accounts for convective, oncotic, and diffusive transport of a molecular solute across the endothelium.[14] Developing a fundamental knowledge of EVP and drug penetration in lymph nodes will greatly contribute to the understanding of lymph node (patho-)physiology and allow for improvement in the treatment of cancer patients with lymph node metastasis.

2 | MATERIALS AND METHODS

2.1 | Mice

All mice were bred and kept in a gnotobiotic animal facility. Approval by the Massachusetts General Hospital Institutional Animal Care and Use Committee was obtained for all experiments. We used 8- to 14-week-old BALB/c male mice (26 *g*–34 *g*). The immunocompetent BALB/c strain was selected for lacking melanin, which can build up in the lymph node over time and cause autofluorescence in pigmented mouse strains (Fig. S1). This autofluorescence may interfere with accurate vessel masking for EVP measurements as described below.

2.2 | Measuring effective vascular permeability using multiphoton microscopy

We performed EVP measurements using multiphoton microscopy[14] on normal lymph node and dorsal skinfold vasculature in twenty-five BALB/c mice. Surgical implantation of the chronic lymph node window and dorsal skinfold chamber was performed under general anesthesia (100/10 mg ketamine/xylazine mixture per kg body weight) as previously described.[18–21] These chronic window models allow for nearly motionless intravital imaging. Two days after surgical implantation, the mouse was positioned on an imaging stage, and a cannula was inserted into the tail vein for intravenous access. Thirty seconds after intravenous injection in the tail vein of 100 μL of a 1% solution of FITC-BSA (Sigma-Aldrich, St. Louis, MO, USA; A9771), imaging was performed using a custom-built multiphoton laser-scanning microscope (adapted from Olympus 300; Optical Analysis Corp., Nashua, NH, USA) with a broadband femtosecond laser source (High Performance MaiTai, Santa Clara, CA, USA, Spectra-Physics). Slowest acquisition (~0.85 sec per slice) on Olympus FluoView software was employed to get best quality images containing 256 × 256 pixels (~482.65 μm × 482.65 μm). Seventy-four *z*-slices starting ~15–20 μm below tissue surface with steps of 1.84 μm were obtained with a 25× 1.05NA water-immersion objective at 1.5× digital zoom (Figure 1). Image slices were acquired with ~60 mW on sample laser power at 780 nm wavelength. For signal detection, we used a 535DF43 emission filter in front of the photomultiplier tube. Using these settings, there is no photobleaching or saturation of the FITC-BSA fluorophore. For each EVP measurement, eight time-lapse image stacks were obtained over a ~16-minute time span. Vessel masking was performed using ImageJ[22] 1.47v image analysis software (NIH): The image stack was converted to binary using the threshold method “Li” followed by a 3D median filter (radius 1 pixel) to remove background single voxel noise. Custom analysis software written in Matlab version r2013a (available in Data S1) is used to calculate the EVP after vessel masking, which is based on the first stack of image slices acquired 30 seconds after FITC-BSA injection. This vessel mask then allows identification of signal intensity changes inside and outside the vessels over time in all stacks of image slices using a 3D box-shaped ROI approach containing multiple vessels as recently described.[14] In short, this box-shaped ROI approach segments the voxels in a data stack into those inside the vessel, those on the vessel wall or those outside the vessel using the vessel masking. For calculating EVP, all vessels combined are mathematically considered as a single vessel. EVP (cm/s) is calculated as $\mathrm{EVP}=\frac{(voxelsize)*\mathrm{Slope\ of}\ F_e\ \mathrm{overtime}}{(n_{\mathrm{wall}})*\mathrm{Mean\ of}\ (F_v-F_i)}$ where *voxel size* is the size of a voxel (ie, 1.84×10^{-6} cm^3),

F_e is total fluorescence from all exterior points including those on the wall, n_{wall} is the number of voxels making up the vessel walls, F_V is the mean fluorescence from the voxels inside the vessel, and F_i is the mean fluorescence of the vessel wall voxels.

For VEGF-A treatment, 8 mg/kg recombinant mouse VEGF-A 164 Protein (R&D Systems, #493-MV-005) in 50 μL of sterile PBS was administered retro-orbitally 2 hours before imaging. For histamine treatment, histamine dihydrochloride 12.5 mg/kg (R&D systems, #3545/50) in 50 μL of sterile PBS was administered intravenously together with FITC-BSA. All mice were euthanized after imaging.

2.3 | High-performance liquid chromatography

For HPLC, a total of sixty-four 8- to 16-week-old BALB/c male mice (four mice per drug per time point) were treated with 50 mg/kg 5-FU (Sigma-Aldrich F6627), 20 mg/kg paclitaxel (ChemieTek, Indianapolis, IN, USA; CT-0502), 20 mg/kg cisplatin (Selleckchem, Houston, TX, USA; S1166), or 10 mg/kg doxorubicin (Selleckchem, S1208). For the time-point evaluation, an additional 24 BALB/c mice were used (2 mice per drug per time point, available in the Data S1). At 10 minutes, 2 hours, 4 hours, 8 hours, and 24 hours, mouse whole blood was collected in an EDTA tube using cardiac puncture and snap-frozen in liquid nitrogen. The liver, spleen, brain, and lymph nodes were snap-frozen in cryovials for subsequent analysis. The mandibular, cranial deep cervical, proper axillary, accessory axillary, subiliac, popliteal, jejunal, colic, and medial iliac lymph nodes[23] were collected and grouped per animal. Up to 200 mg of organ tissues was separately weighed and homogenized in 1 mL CelLytic™ tissue lysis buffer (Sigma-Aldrich C3228) on ice for at least 1 minute until complete decomposition of the bulk tissue. 500 μL of cold methanol was added to 500 μL of the homogenate, vortexed, and then centrifuged at 14 600 *g* for 10 minutes (5415D Microcentrifuge, Eppendorf, Hauppauge, NY, USA). The supernatant was collected, and the pellet discarded. In addition, 5-FU and doxorubicin were extracted with 5 mL ethyl acetate, vortexed for 1 minute, and centrifuged for 10 minutes. The organic layer was collected and evaporated to dryness using Genevac EZ-2 (SP Scientific, Warminster, PA, USA). The dry pellet was reconstituted with 500 μL of deionized water. To measure the concentration of drugs in the homogenate sample, 500 μL of the supernatant solution (for paclitaxel and cisplatin) or deionized water (for 5-FU and doxorubicin) was filtered through a 0.22 μm centrifuge filter (Sigma-Aldrich, CLS8161). The solution was then transferred into an HPLC vial and analyzed by HPLC (Atlantics dC18 column, 250 mm × 4.6 mm, i.d. 5 μm).

2.4 | Immunohistochemistry

For visualization of histamine receptor on the vascular endothelium of the lymph node, we used goat anti-mouse HRH1 antibody (Santa Cruz Biotechnology, Dallas, TX, USA; sc-20633, 1:50) and rat anti-mouse MECA-32 (BD, 553849, 1:100) on paraffin-embedded BALB/c lymph node tissue sections (5 μm thickness). Donkey anti-mouse IgM-488 and IgM-cy3 were used as secondary antibodies (1:250) for HRH1 and MECA-32, respectively.

2.5 | Statistics

Graphpad Prism v7.02 was used for all statistical analyses. For comparisons between two groups, an unpaired nonparametric Mann-Whitney *t* test was performed. For analysis of multiple groups, a Kruskal-Wallis ANOVA was performed with Dunn's multiple comparisons test. Results are presented as Mean ± SEM.

3 | RESULTS

3.1 | Effective vascular permeability in lymph nodes

Using our methods, we measured a mean EVP (Figure 1) in normal lymph node blood vessels of $9.9 \pm 1.5 \times 10^{-8}$ cm/s (n=7) in BALB/c mice. We found that normal lymph node blood vessel EVP was not significantly different compared to untreated subcutaneous blood vessels. Next, we evaluated whether lymph node EVP could be increased by using murine histamine (12.5 mg/kg) and VEGF-A (8 mg/kg), as both have been shown to cause rapid increases in vascular permeability.[24,25] We verified the presence of HRH1 on lymph node blood vessel endothelium (Fig. S2). Dunn's multiple comparisons test demonstrated that the EVP of lymph nodes treated with histamine (n=5, $4.1 \pm 0.9 \times 10^{-7}$ cm/s) and VEGF-A (n=8, $3.8 \pm 0.7 \times 10^{-7}$ cm/s) was significantly greater than untreated lymph nodes (Figure 1). Using these doses, we showed that blood vessel EVP can be increased ~fourfold in lymph nodes.

3.2 | Chemotherapy penetration in untreated and VEGF-A-treated lymph nodes

Next, we tested whether an increase in lymph node EVP could lead to an increased accumulation of chemotherapeutic drugs. We selected commonly used chemotherapeutic drugs from different classes and with variable drug properties (Table 1) and compared drug accumulation in untreated and VEGF-A-treated mice 2 hours and 4 hours (n=4 per group) after a single chemotherapeutic drug injection (Figure 2). HPLC drug calibration curves showed good correlation to drug standards (R^2 >.99, Fig. S3), and there was no false-positive signal in untreated tissue for any of the drugs. Time points were chosen based on the maximum lymph node drug concentration of 5-FU and paclitaxel (Fig. S4). The absence of signal for 5-FU and paclitaxel in tissues and blood in uninjected animals are shown in Fig. S4. Cisplatin and doxorubicin levels were also not detectable in uninjected animals (not shown). On average per mouse, 962 μL, 35 mg, 1269 mg, 96 mg, and 440 mg of blood, lymph node, liver, spleen, and brain tissue were harvested, respectively. Dunn's multiple comparisons test was performed for all comparisons. There were no significant differences in drug concentration in the brains of animals treated with VEGF-A relative to control, and as expected, all values were low compared to blood. Mean blood cisplatin concentrations were significantly lower after 2 hours in VEGF-A-treated animals compared to control. Spleen and liver showed no significant changes with VEGF-A treatment. In lymph nodes, doxorubicin had the highest drug concentration, despite having the lowest injected dose at 10 mg/kg. For all drugs, no significant difference in lymph node drug concentration was observed after administration of VEGF-A. When comparing untreated lymph node to liver at 2 hours and 4 hours using an unpaired t test, 5-FU and paclitaxel concentrations were significantly lower in lymph node at 4 hours. Surprisingly, increasing EVP by administering VEGF-A did not increase maximum lymph node drug penetration.

4 | DISCUSSION

The efficacy of chemotherapy on isolated metastatic cancer cells or micrometastases in the lymph node may depend on the ability of chemotherapeutic drugs to reach its target in therapeutic concentrations. Therefore, we tested whether maximum chemotherapeutic drug concentrations could be increased in lymph nodes by increasing blood vessel EVP. We found that blood vessel EVP can be increased in lymph nodes by administering VEGF-A systemically. However, this did not increase maximum drug concentrations in any organ tested.

We first analyzed the EVP in normal, untreated blood vessels in lymph nodes, and in the dorsal skinfold chamber in BALB/c mice. The latter was performed to compare blood vessel EVP measurements made using our novel 3D method, to published measurements of FITC-BSA EVP in the same dorsal skinfold chamber surgical preparation using a 2D method[14] (Table 2). Normal subcutaneous blood vessels using this 2D method were found to have an EVP around 5.0×10^{-8} cm/s and 7.5×10^{-8} cm/s in SCID and C57BL/6 mice, respectively.[26,27] EVP measured in SCID mouse normal pancreas[28] and brain[26] was found to be similar to SCID subcutaneous blood vessels (~5.0×10^{-8} cm/s), while normal liver blood vessel EVP was lower (2.7×10^{-8} cm/s).[29] Our EVP measurements using a 3D approach in immunocompetent BALB/c mice are twofold higher (n=5, $1.6 \pm 0.4 \times 10^{-7}$ cm/s) than what was reported in immunocompetent C57BL/6 mice, most likely attributable to the reduced (and less accurate) blood vessel volume estimation resulting from the 2D approach. These measurements in SCID mice also suggest mouse strain as a source of variation.

No significant differences in drug accumulation were measured in the lymph nodes of VEGF-A treated animals relative to untreated controls. There was variability in some measurements, which could not be explained by HPLC inaccuracy as all HPLC drug calibration curves had an R^2 >.99, and no false-positive signal could be detected (Fig. S3). Therefore, the variability was likely due to experimental variability, which could arise from unforeseen variation between animals, including the amount of lymph flow through individual lymph nodes that could lead to drug washout. The brain was harvested to serve as a negative control and, as expected, produced a low signal for doxorubicin[30] and 5-FU.[31] Very little to no signal for paclitaxel[32] and cisplatin[33] was detected in the brain. Interestingly, lymph node paclitaxel penetration was significantly reduced compared to liver at the 2 hours time point, and absent at the 10 minute time point (Fig. S4), suggesting a slower drug uptake of paclitaxel in the lymph node. It is unclear from our data whether this is related to the lipophilicity of paclitaxel.

Lymph enters the lymph node via afferent lymphatic vessels to the lymph node subcapsular sinus. It is known that smaller molecules up to an approximate molecular weight of 70 kDa[34–36] from the lymph are found in lymph node conduits, penetrate more deeply, and enter the lymph node B- or T-cell zones. Subcapsular macrophages and dendritic cells are known to transfer larger molecules (>70 kDa) from the sub-capsular sinus to more superficial B cells.[35,37–39] However, molecular delivery to the lymph node from the blood is

not well understood, and the exact lymph node blood vessel and high endothelial venule pore cut-off sizes are, to our knowledge, unknown.

Molecules roughly 5 nm or larger are usually impermeable to the blood capillaries within healthy nonlymphoid tissues.[40] HSA is a negatively charged molecule, 3.8 nm in diameter, 15 nm long, and ~69 kDa[41] in size. HSA binds paclitaxel and cisplatin (>95%), to a lesser extent doxorubicin (~75%), and some of their degraded products, changing total molecule size and extending plasma half-life.[42–45] HSA binds weakly to 5-FU.[46] Based on our findings that VEGF-A increased lymph node blood vessel EVP to FITC-BSA (~67 kDa in size), we expected that VEGF-A pretreatment would allow more HSA bound paclitaxel, cisplatin and doxorubicin to enter the lymph node and increase maximum drug concentrations. We also hypothesized 5-FU would better penetrate the lymph node than any of the other drugs even without VEGF-A treatment, as it has a much weaker binding to HSA.[46] Doxorubicin, however, exceeded 5-FU drug penetration in all organs, likely as a result of the short plasma half-life of 5-FU[47] which resulted in low blood concentrations at the selected time points.

Adair et al.[48–50] describe experimental settings in dog popliteal lymph nodes where, under physiologic pressures, 10% of the afferent lymph fluid (not protein) was absorbed by blood vessels in the lymph node. The validity of their findings is strengthened by other data where dog popliteal lymph node blood vessels absorbed up to 50% of fluid in some settings.[51] Protein concentrations under normalized conditions were higher in the efferent lymph vessel than the afferent lymphatic vessels, attributable to protein leaving the blood and net fluid getting absorbed by the blood.[50] Using computational modeling, Jafarnejad et al.,[52] showed most fluid in the lymph node subcapsular sinus is hypothesized to travel to the medullary sinuses and leave the node via the efferent lymphatic vessel, following the path of least resistance. These data are supported by Kourtis et al.,[53] where after peripheral nanoparticle injection, the particles pass the lymph node mostly through the subcapsular sinus. Only approximately 7% of all fluid entering the lymph node reaches the center of the lymph node and is expected to leave through blood vessels under physiological pressures.[52] Fluid flux through the lymph node[52] can also cause wash-out of drugs, which may dominate vascular permeability as the main determinate of drug accumulation. Any drug in the subcapsular or medullary sinuses is likely to be washed out by lymph flow more easily.

Our measurement method for effective vascular permeability accounts for all processes that move material from the blood vessels to the extravascular space in the center of the lymph node based on FITC-BSA, which pertains to similarly sized HSA-bound chemotherapy. This being said, we are not measuring vascular permeability of fluid, but an effective vascular permeability of FITC-BSA that accounts for net transport effects of diffusive, convective, and oncotic forces. While centralized fluid is expected to leave through blood vessels in the lymph node in the physiologic setting,[48–50] protein (like albumin) is not expected to.[50] Hence, data in the literature and our effective vascular permeability measurements argue against net protein transport from the lymph node to the blood, but fluid transport can occur in this direction. What happens to other macromolecules and free drug is less clear. Regardless, increasing blood vessel permeability is postulated to decrease or reverse lymph to blood exchange in the lymph node center[52] and promote transport out of the blood.

However, drug accumulation did not increase with increased EVP. Thus, a possible explanation for our findings is that VEGF-A increased fluid flow through the lymph node, which carried the drug out of the lymph node toward efferent lymphatic vessels.

Solas et al.[11] evaluated protease inhibitor concentrations in lymph nodes of patients infected with HIV. Differential penetration into lymphoid tissue was observed, with average lymph node tissue/plasma concentration ratios 4–8 hours after drug intake of 2.07, 0.64, 0.58, and 0.21 for the highly lipophilic drugs indinavir, ritonavir, nelfinavir, and lopinavir, respectively. All 41 patients in the study had detectable HIV-1 RNA in lymph node biopsies, while 13 patients had detectable HIV-1 RNA in plasma, indicating that the ratios were at subtherapeutic levels in these patients. Significantly reduced levels of antiretroviral drug penetration of lymphoid tissue compared to plasma have also been measured in animal models.[9,54,55] In our study, we calculated average lymph node tissue/plasma concentration ratios at 4 hours for 5-FU, paclitaxel, cisplatin, and doxorubicin of 1.5, 0.09, 0.09, and 0.5, respectively. After VEGF-A treatment, the ratio was significantly increased only for paclitaxel (average ratio 0.35 ± 0.07, P=.035). It is unclear however, whether it is low drug concentration in the lymph node that causes therapy failure, or whether certain lymph node regions provide protection for metastatic cancer cells and HIV-infected T cells. B-cell follicles specifically have been shown to constitute sanctuaries for persistent HIV and SIV (HIV nonhuman primate counterpart) infections.[13,56] More research is needed to evaluate whether what has been learned from HIV studies can be applied to the treatment of lymph node metastasis. However, from our findings, we hypothesize that increasing lymph node blood vessel EVP is unlikely to increase therapy effectiveness of the tested chemotherapy drugs without changing their drug properties or reducing drug washout by inhibiting lymph flow.

The present study has limitations. Our goal was to evaluate whether we could increase maximum drug concentration in the lymph node. Therefore, we evaluated the time points (10 minutes, 2 hours, 4 hours, 8 hours, and 24 hours) that yielded the highest lymph node drug concentration using 5-FU and paclitaxel (Fig. S4). We moved forward with the 2 hour and 4 hour time points, accepting that the area under the curve cannot be calculated from solely these time points. Hence, complete evaluation of chemotherapeutic drug penetration during a dosing interval and the pharmacokinetic properties of the respective drugs with or without VEGF-A treatment were not evaluated. In addition, HPLC might not be sensitive enough to detect a small change in drug concentration. Regardless, we could detect drug in all samples, supported by a linear calibration curve even in the low concentration range (Fig. S3). VEGF-A increased effective vascular permeability ~fourfold, and a comparable (orlesser) change in drug accumulation could be easily detected; therefore, we believe the technique is capable of detecting major and biologically relevant changes. Moreover, some loss of drug could have occurred in processing, although it was not biased to any particular sample, and all relative comparisons are valid. We cannot exclude that the absolute values of drug may underestimate the true tissue concentration. In addition, our study is performed in lymph nodes not harboring metastatic cancer cells. It is known that prior to cancer cell dissemination, tumor-draining lymph nodes may undergo many remodeling processes including lymph node lymphangiogenesis, remodeling of high endothelial venules, alterations in immune cell populations and changes in chemokines and cytokines

expression.[7] We hypothesize that these changes might not be as robust in the settings of isolated metastatic cancer cells. However, in the pre- and micrometastatic setting, changes in conduits and angiogenesis are not reported,[20] both of which play a role in molecular transport in lymph nodes. Future evaluation of lymph node blood vessel EVP in the setting of lymph nodes harboring isolated metastatic cancer cells would allow further characterization of chemotherapy penetration in lymph nodes. Lastly, the intravital multiphoton microscopy imaging field of view is limited in x, y, and z (~483 × 483 × 136 μm).[14] Therefore, while the HPLC analysis of lymph nodes was performed on complete lymph nodes, the imaging described for evaluation of blood vessel EVP predominantly included the cortical region of the lymph node.

Globally increasing permeability by using systemic treatments causes drug to accumulate in other organs, arguably even more than in lymph nodes. Specific lymph node targeting would be a promising approach. There are some techniques that target the lymphatic system more specifically by lymphatic drainage. Recent literature[8,53] describes direct lymph node injection and subcutaneous injections of synthetic materials, biopolymers (eg, albumin), and nanoparticles. Recent work on endogenous cell-mediated trafficking is also described, employing antigen-presenting cells to target lymphoid organs. Alternatively, therapies to impair lymphatic vessel function can be systemically administered to prevent washout from the lymph nodes by lymph flow, and methods can be developed to measure lymph node drug efflux. Thus, there are multiple approaches which could be employed in future research to help improve drug accumulation in lymph nodes.

In conclusion, here we report measurements of EVP of lymph node blood vessels for the first time as an initial step to understanding the ability of systemic drugs to penetrate and accumulate in lymph nodes. As our basic understanding grows, we hope to exploit our findings to improve the therapeutic efficiency of drugs treating disease in lymph nodes.

5 | PERSPECTIVES

We report here the first measurements of effective vascular permeability of lymph node blood vessels. No significant differences in lymph node chemotherapeutic drug concentration were observed after increasing the effective vascular permeability of lymph node blood vessels. We hypothesize that these findings may be explained by fluid flow through the lymph node that causes drug washout. The investigation of alternative drug properties and measuring or altering lymph node drug efflux are promising areas of research to improve drug accumulation in lymph nodes.

Supplementary Material

Refer to Web version on PubMed Central for supplementary material.

Acknowledgments

Research reported in this publication was supported in part by the National Institutes of Health under award numbers DP2OD008780 (T.P.P.), R01HL128168 (J.W.B., T.P.P.), R01CA214913 (T.P.P.), R01CA163528 (B.J.V.), F32CA183465 (D.J.), the UNCF-Merck Science Initiative Postdoctoral Fellowship (D.J.), the Burroughs Wellcome Fund Postdoctoral Enrichment Program Award (D.J.), and the National Cancer Institute Federal Share of Proton

Income CA059267 (T.P.P.). The Center for Biomedical OCT Research and Translation also supported this work through Grant Number P41EB015903, awarded by the National Institute of Biomedical Imaging and Bioengineering of the National Institutes of Health. C.B. was supported by a Swiss National Science Foundation early postdoctoral mobility fellowship (P2SKP2_158640).

Funding information

National Institutes of Health, Grant/Award Number: DP2OD008780, R01HL128168, R01CA214913, R01CA163528 and F32CA183465; National Cancer Institute, Grant/Award Number: CA059267; National Institutes of Health, Grant/Award Number: P41EB015903; Swiss National Science Foundation, Grant/Award Number: P2SKP2_158640

Abbreviations

2D	Two-dimensional
3D	Three-dimensional
5-FU	5-fluorouracil
DAPI	4′,6-diamidino-2-phenylindole
EDTA	Ethylenediamine tetraacetic acid
EVP	Effective vascular permeability
FITC-BSA	Fluorescein isothiocyanate conjugated to bovine serum albumin
HIV	Human immunodeficiency virus
HPLC	High-performance liquid chromatography
HRH1	Histamine H1 receptor
HSA	Human serum albumin
LN	Lymph node
MECA-32	Mouse endothelial cell antigen-32
PBS	Phosphate buffered saline
ROI	region of interest
SCID	severe combined immunodeficiency
SEM	Standard error of mean
SIV	Simian immunodeficiency virus
VEGF-A	Vascular endothelial growth factor A

References

1. Kawada K, Taketo MM. Significance and mechanism of lymph node metastasis in cancer progression. Cancer Res. 2011; 71:1214–1218. [PubMed: 21212413]

2. Vakoc BJ, Lanning RM, Tyrrell JA, et al. Three-dimensional microscopy of the tumor microenvironment in vivo using optical frequency domain imaging. Nat Med. 2009; 15:1219–1223. [PubMed: 19749772]

3. Jain RK. Normalizing tumor microenvironment to treat cancer: bench to bedside to biomarkers. J Clin Oncol. 2013; 31:2205–2218. [PubMed: 23669226]

4. Padera TP, Kuo AH, Hoshida T, et al. Differential response of primary tumor versus lymphatic metastasis to VEGFR-2 and -3 kinase inhibitors cediranib and vandetanib. Mol Cancer Ther. 2008; 7:2272–2279. [PubMed: 18687659]

5. Eichler AF, Chung E, Kodack DP, Loeffler JS, Fukumura D, Jain RK. The biology of brain metastases—translation to new therapies. Nat Rev Clin Oncol. 2011; 8:344–356. [PubMed: 21487419]

6. Straver ME, Rutgers EJ, Russell NS, et al. Towards rational axillary treatment in relation to neoadjuvant therapy in breast cancer. Eur J Cancer. 2009; 45:2284–2292. [PubMed: 19464164]

7. Pereira ER, Jones D, Jung K, Padera TP. The lymph node microenvironment and its role in the progression of metastatic cancer. Semin Cell Dev Biol. 2015; 38:98–105. [PubMed: 25620792]

8. Thomas SN, Schudel A. Overcoming transport barriers for interstitial-, lymphatic-, and lymph node-targeted drug delivery. Curr Opin Chem Eng. 2015; 7:65–74. [PubMed: 25745594]

9. Bourry O, Mannioui A, Sellier P, et al. Effect of a short-term HAART on SIV load in macaque tissues is dependent on time of initiation and antiviral diffusion. Retrovirology. 2010; 7:78. [PubMed: 20868521]

10. Cory TJ, Schacker TW, Stevenson M, Fletcher CV. Overcoming pharmacologic sanctuaries. Curr Opin HIV AIDS. 2013; 8:190–195. [PubMed: 23454865]

11. Solas C, Lafeuillade A, Halfon P, Chadapaud S, Hittinger G, Lacarelle B. Discrepancies between protease inhibitor concentrations and viral load in reservoirs and sanctuary sites in human immunodeficiency virus-infected patients. Antimicrob Agents Chemother. 2003; 47:238–243. [PubMed: 12499197]

12. Freeling JP, Ho RJ. Anti-HIV drug particles may overcome lymphatic drug insufficiency and associated HIV persistence. Proc Natl Acad Sci USA. 2014; 111:E2512–E2513. [PubMed: 24889644]

13. Fukazawa Y, Lum R, Okoye AA, et al. B cell follicle sanctuary permits persistent productive simian immunodeficiency virus infection in elite controllers. Nat Med. 2015; 21:132–139. [PubMed: 25599132]

14. Meijer EF, Baish JW, Padera TP, Fukumura D. Measuring vascular permeability in vivo. Methods Mol Biol. 2016; 1458:71–85. [PubMed: 27581015]

15. Carmeliet P, Jain RK. Molecular mechanisms and clinical applications of angiogenesis. Nature. 2011; 473:298–307. [PubMed: 21593862]

16. Senger DR, Galli SJ, Dvorak AM, Perruzzi CA, Harvey VS, Dvorak HF. Tumor cells secrete a vascular permeability factor that promotes accumulation of ascites fluid. Science. 1983; 219:983–985. [PubMed: 6823562]

17. Azzi S, Hebda JK, Gavard J. Vascular permeability and drug delivery in cancers. Front Oncol. 2013; 3:211. [PubMed: 23967403]

18. Leunig M, Yuan F, Menger MD, et al. Angiogenesis, microvascular architecture, microhemodynamics, and interstitial fluid pressure during early growth of human adenocarcinoma LS174T in SCID mice. Cancer Res. 1992; 52:6553–6560. [PubMed: 1384965]

19. Brown E, Munn LL, Fukumura D, Jain RK. In vivo imaging of tumors. Cold Spring Harb Protoc. 2010; 2010 pdb.prot5452.

20. Jeong HS, Jones D, Liao S, et al. Investigation of the lack of angiogenesis in the formation of lymph node metastases. J Natl Cancer Inst. 2015; 107:djv155. [PubMed: 26063793]

21. Meijer EFJ, Jeong HS, Pereira ER, et al. Murine chronic lymph node window for longitudinal intravital lymph node imaging. Nat Protoc. 2017; 12:1513–1520. [PubMed: 28683064]

22. Rasband, WS. ImageJ. U. S. National Institutes of Health; Bethesda, Maryland, USA: 1997–2017. http://rsb.info.nih.gov/ij/ [Accessed May 14, 2016]

23. Van den Broeck W, Derore A, Simoens P. Anatomy and nomenclature of murine lymph nodes: descriptive study and nomenclatory standardization in BALB/cAnNCrl mice. J Immunol Methods. 2006; 312:12–19. [PubMed: 16624319]
24. Feng D, Nagy JA, Hipp J, Dvorak HF, Dvorak AM. Vesiculo-vacuolar organelles and the regulation of venule permeability to macromolecules by vascular permeability factor, histamine, and serotonin. J Exp Med. 1996; 183:1981–1986. [PubMed: 8642308]
25. Dellian M, Witwer BP, Salehi HA, Yuan F, Jain RK. Quantitation and physiological characterization of angiogenic vessels in mice: effect of basic fibroblast growth factor, vascular endothelial growth factor/vascular permeability factor, and host microenvironment. Am J Pathol. 1996; 149:59–71. [PubMed: 8686763]
26. Monsky WL, Fukumura D, Gohongi T, et al. Augmentation of transvascular transport of macromolecules and nanoparticles in tumors using vascular endothelial growth factor. Cancer Res. 1999; 59:4129–4135. [PubMed: 10463618]
27. Fukumura D, Gohongi T, Kadambi A, et al. Predominant role of endothelial nitric oxide synthase in vascular endothelial growth factor-induced angiogenesis and vascular permeability. Proc Natl Acad Sci USA. 2001; 98:2604–2609. [PubMed: 11226286]
28. Tsuzuki Y, Mouta CC, Bockhorn M, Xu L, Jain RK, Fukumura D. Pancreas microenvironment promotes VEGF expression and tumor growth: novel window models for pancreatic tumor angiogenesis and microcirculation. Lab Inves. 2001; 81:1439–1451.
29. Fukumura D, Yuan F, Monsky WL, Chen Y, Jain RK. Effect of host microenvironment on the microcirculation of human colon adenocarcinoma. Am J Pathol. 1997; 151:679–688. [PubMed: 9284816]
30. Sardi I, la Marca G, Cardellicchio S, et al. Pharmacological modulation of blood-brain barrier increases permeability of doxorubicin into the rat brain. Am J Cancer Res. 2013; 3:424–432. [PubMed: 23977451]
31. Lin NU, Bellon JR, Winer EP. CNS metastases in breast cancer. J Clin Oncol. 2004; 22:3608–3617. [PubMed: 15337811]
32. Fellner S, Bauer B, Miller DS, et al. Transport of paclitaxel (Taxol) across the blood-brain barrier in vitro and in vivo. J Clin Investig. 2002; 110:1309–1318. [PubMed: 12417570]
33. Minami T, Okazaki J, Kawabata A, Kuroda R, Okazaki Y. Penetration of cisplatin into mouse brain by lipopolysaccharide. Toxicology. 1998; 130:107–113. [PubMed: 9865478]
34. Gretz JE, Norbury CC, Anderson AO, Proudfoot AE, Shaw S. Lymph-borne chemokines and other low molecular weight molecules reach high endothelial venules via specialized conduits while a functional barrier limits access to the lymphocyte microenvironments in lymph node cortex. J Exp Med. 2000; 192:1425–1440. [PubMed: 11085745]
35. Sixt M, Kanazawa N, Selg M, et al. The conduit system transports soluble antigens from the afferent lymph to resident dendritic cells in the T cell area of the lymph node. Immunity. 2005; 22:19–29. [PubMed: 15664156]
36. Nolte MA, Belien JA, Schadee-Eestermans I, et al. A conduit system distributes chemokines and small blood-borne molecules through the splenic white pulp. J Exp Med. 2003; 198:505–512. [PubMed: 12900524]
37. Roozendaal R, Mempel TR, Pitcher LA, et al. Conduits mediate transport of low-molecular-weight antigen to lymph node follicles. Immunity. 2009; 30:264–276. [PubMed: 19185517]
38. Phan TG, Grigorova I, Okada T, Cyster JG. Subcapsular encounter and complement-dependent transport of immune complexes by lymph node B cells. Nat Immunol. 2007; 8:992–1000. [PubMed: 17660822]
39. Carrasco YR, Batista FD. B cells acquire particulate antigen in a macrophage-rich area at the boundary between the follicle and the sub-capsular sinus of the lymph node. Immunity. 2007; 27:160–171. [PubMed: 17658276]
40. Kaminskas LM, Kota J, McLeod VM, Kelly BD, Karellas P, Porter CJ. PEGylation of polylysine dendrimers improves absorption and lymphatic targeting following SC administration in rats. J Control Release. 2009; 140:108–116. [PubMed: 19686787]
41. Gekle M. Renal tubule albumin transport. Annu Rev Physiol. 2005; 67:573–594. [PubMed: 15709971]

42. Purcell M, Neault JF, Tajmir-Riahi HA. Interaction of taxol with human serum albumin. Biochem Biophys Acta. 2000; 1478:61–68. [PubMed: 10719175]
43. Neault JF, Tajmir-Riahi HA. Interaction of cisplatin with human serum albumin. Drug binding mode and protein secondary structure. Biochem Biophys Acta. 1998; 1384:153–159. [PubMed: 9602104]
44. Agudelo D, Berube G, Tajmir-Riahi HA. An overview on the delivery of antitumor drug doxorubicin by carrier proteins. Int J Biol Macromol. 2016; 88:354–360. [PubMed: 27037051]
45. Barakat, RR., Markman, M., Randall, ME. Principles and Practice of Gynecologic Oncology. 5. Philadelphia: Wolters Kluwer Lippincott Williams & Wilkins; 2009. p. 386
46. Bertucci C, Ascoli G, Uccello-Barretta G, Di Bari L, Salvadori P. The binding of 5-fluorouracil to native and modified human serum albumin: UV, CD, and 1H and 19F NMR investigation. J Pharm Biomed Anal. 1995; 13:1087–1093. [PubMed: 8573632]
47. Bocci G, Danesi R, Di Paolo AD, et al. Comparative pharmacokinetic analysis of 5-fluorouracil and its major metabolite 5-fluoro-5,6-dihydrouracil after conventional and reduced test dose in cancer patients. Clin Cancer Res. 2000; 6:3032–3037. [PubMed: 10955781]
48. Adair TH, Guyton AC. Modification of lymph by lymph nodes. II. Effect of increased lymph node venous blood pressure. Am J Physiol. 1983; 245:H616–H622. [PubMed: 6624930]
49. Adair TH, Guyton AC. Modification of lymph by lymph nodes. III. Effect of increased lymph hydrostatic pressure. Am J Physiol. 1985; 249:H777–H782. [PubMed: 4051014]
50. Adair TH, Moffatt DS, Paulsen AW, Guyton AC. Quantitation of changes in lymph protein concentration during lymph node transit. Am J Physiol. 1982; 243:H351–H359. [PubMed: 7114267]
51. Knox P, Pflug JJ. The effect of the canine popliteal node on the composition of lymph. J Physiol. 1983; 345:1–14. [PubMed: 6663494]
52. Jafarnejad M, Woodruff MC, Zawieja DC, Carroll MC, Moore JE Jr. Modeling lymph flow and fluid exchange with blood vessels in lymph nodes. Lymphat Res Biol. 2015; 13:234–247. [PubMed: 26683026]
53. Kourtis IC, Hirosue S, de Titta A, et al. Peripherally administered nanoparticles target monocytic myeloid cells, secondary lymphoid organs and tumors in mice. PLoS ONE. 2013; 8:e61646. [PubMed: 23626707]
54. Horiike M, Iwami S, Kodama M, et al. Lymph nodes harbor viral reservoirs that cause rebound of plasma viremia in SIV-infected macaques upon cessation of combined antiretroviral therapy. Virology. 2012; 423:107–118. [PubMed: 22196013]
55. North TW, Higgins J, Deere JD, et al. Viral sanctuaries during highly active antiretroviral therapy in a nonhuman primate model for AIDS. J Virol. 2010; 84:2913–2922. [PubMed: 20032180]
56. Deleage C, Wietgrefe SW, Del Prete G, et al. Defining HIV and SIV reservoirs in lymphoid tissues. Pathog Immun. 2016; 1:68–106. [PubMed: 27430032]

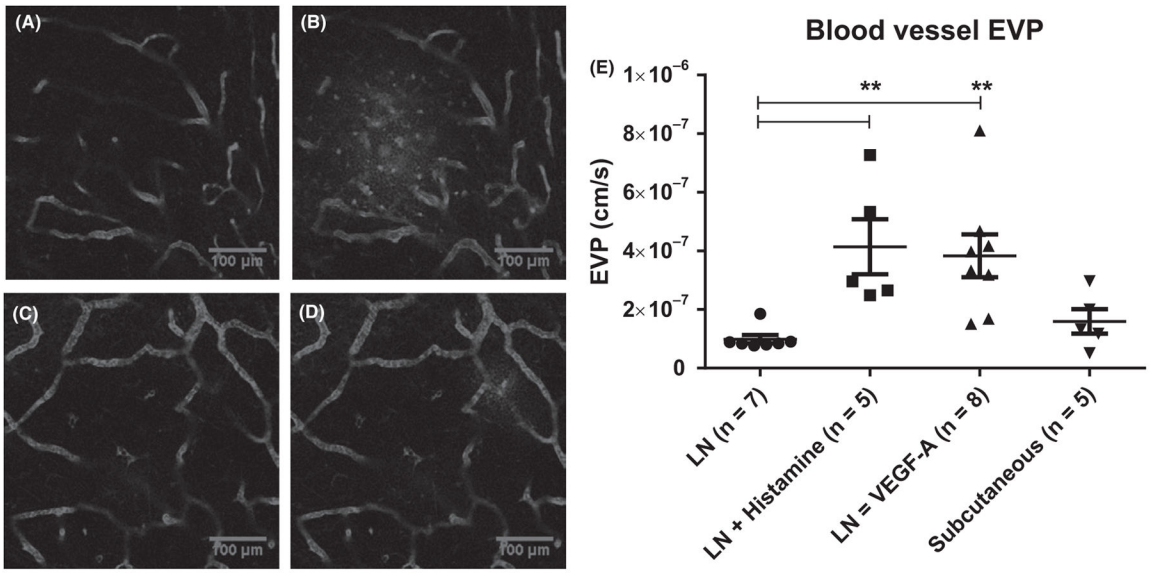

FIGURE 1.

Blood vessel effective vascular permeability. (A) Intravital multiphoton microscopy demonstrates the presence of FITC-BSA in lymph node blood vasculature of a BALB/c mouse ~ 30 seconds after intravenous injection. (B) Image of the same location as A, ~14 minutes later shows FITC-BSA extravasation is most apparent in left side. C–D) Images at 30 s (C) and 14 min (D) after injection show extravasation of FITC-BSA in the interstitial space after VEGF-A treatment in different BALB/c mouse with extravasation most apparent in the top right corner. (E) EVP measurements performed in normal, histamine-treated and VEGF-A-treated lymph nodes, as well as subcutaneous blood vessels. Mean and SEM are reported. ** = $P<.01$ using Dunn's multiple comparisons test (ANOVA)

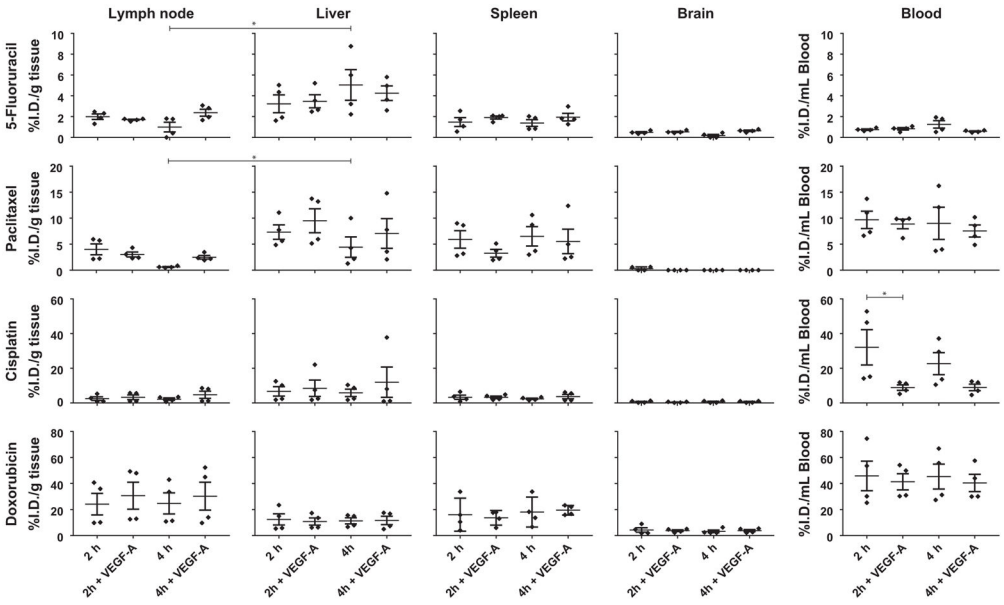

FIGURE 2.

Chemotherapeutic drug concentrations in normal and VEGF-A treated lymph nodes. This figure shows data for all measured chemotherapeutic drugs (5-FU, paclitaxel, cisplatin, and doxorubicin) at 2 hours and 4 h after drug injection, with and without VEGF-A treatment. N=4 per group, mean, and SEM are reported. * = P<.05 using an unpaired nonparametric Mann-Whitney *t* test or Dunn's multiple comparisons test (ANOVA)

TABLE 1

Chemotherapeutic drug properties

	Molecular weight (Da)	Lipophilicity	Charge
5-FU	130	Low	Negative
Paclitaxel	854	High	Negative
Cisplatin	300	Low	Neutral
Doxorubicin	580	Low	Positive

TABLE 2

Summary of effective vascular permeability measurements in mice employing FITC-BSA in a 2D or 3D method

Site	Strain	*2D* Method	*3D* Method	References
Brain	SCID	~5.0×10^{-8} cm/s		23
Liver	SCID	~2.7×10^{-8} cm/s		26
Pancreas	SCID	~5.0×10^{-8} cm/s		25
Subcutaneous blood vessels	SCID	~5.0×10^{-8} cm/s		23
Subcutaneous blood vessels	C57BL/6	~7.5×10^{-8} cm/s		24
Subcutaneous blood vessels	BALB/c		$1.6 \pm 0.4 \times 10^{-7}$ cm/s	
Lymph node	BALB/c		$9.9 \pm 1.5 \times 10^{-8}$ cm/s	
Lymph node + Histamine	BALB/c		$4.1 \pm 0.9 \times 10^{-7}$ cm/s	
Lymph node + VEGF-A	BALB/c		$3.8 \pm 0.7 \times 10^{-7}$ cm/s	